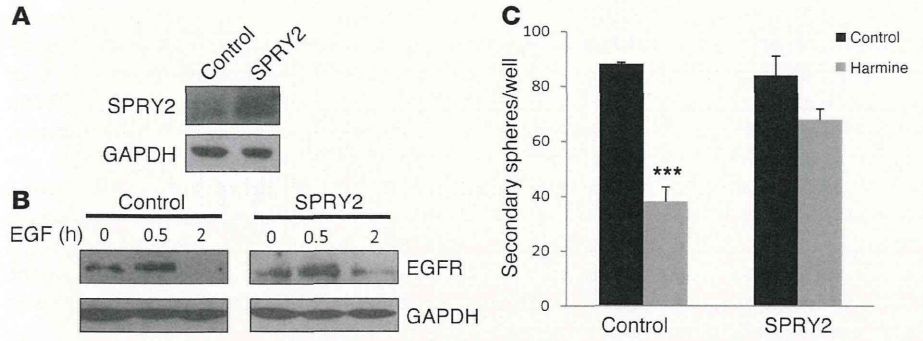

Figure 8

SPRY2 overexpression reverses the effect of harmine on EGFR degradation and GBM-TIC self-renewal. (**A**) GBM5-TICs were infected with control or SPRY2-expressing retrovirus and 48 hours later, the cells were analyzed by Western blotting. (**B**) Control or SPRY2-expressing GBM5-TICs were deprived of growth factors for 12 hours and then EGF was added in the presence of harmine for the indicated durations. EGFR in the cells was analyzed by Western blotting. (**C**) Twenty-four hours after retroviral infection of GBM5-TICs, the cells were incubated in the presence or absence of harmine for 3 days. Dissociated cells were plated in the absence of the drug, and the number of secondary spheres formed was counted. ***$P \leq 0.001$.

GBM-TIC lines (GBM3) that loses EGFR gene amplification and protein expression after long-term culture (without other major genomic changes) (Figure 6H and data not shown), a phenomenon that has been documented in other primary GBM cultures (36). Interestingly, the self-renewal capacity of low-passage GBM3 cells was inhibited in the presence of harmine, although no significant changes were observed in high-passage EGFR-negative cells (Figure 6H). These data concur with our previous observation that shDYRK1A did not inhibit clonal growth of LN18 cells, which do not express EGFR at the membrane (Figure 1A). It also suggests that the main effect of DYRK1A inhibition in GBM cells is mediated through EGFR regulation.

DYRK1A controls EGFR turnover in GBM-TICs. DYRK1A interference appears to diminish the amount of EGFR protein without affecting mRNA levels and, indeed, harmine incubation accelerated receptor degradation in the presence of EGF in SVZ-NSCs (Figure 7A), consistent with our earlier observations (28). Therefore, we checked whether this mechanism was conserved in GBM cells. Both DYRK1A interference (Supplemental Figure 8) and pharmacological inhibition (Figure 7, B and C) accelerated the rate of EGFR degradation following EGF stimulation in the presence of cycloheximide. In agreement with these results, there was a clear increase in the amount of receptors targeted to lysosomes after EGF induction in harmine-treated cells as opposed to that seen in untreated GBM cells (Figure 7D). Intriguingly, expression of the nonlysosomal-targeted EGFRvIII isoform in U87 cells could not rescue the inhibition of EGFR signaling (Supplemental Figure 9A) or the suppression of self-renewal induced by harmine (Supplemental Figure 9B). This suggests that even in the presence of the mutation, GBM self-renewal depends on full-length receptor signaling, as suggested previously (37). In addition, exposure of GBM-TICs to harmine favored the termination of EGFR signaling, though with some differences between GBM lines, which appear to depend on their genetic background. For instance, harmine mainly affected AKT phosphorylation kinetics in the GBM4 line, whereas in the PTEN-deficient GBM5 line, the kinetics of phospho-ERK1/ERK2 was affected, with no clear effect on AKT activation (Figure 7C). These results indicate that DYRK1A inhibition alters the duration of EGFR signaling and suggest that the kinetics of EGFR turnover determines GBM behavior.

SPRY2 overexpression reverses the effect of DYRK1A inhibition on EGFR stability and GBM-TIC self-renewal. The mechanism of DYRK1A action appears to be similar in normal NSCs and GBM-TICs. We previously demonstrated that DYRK1A promoted EGFR stability in NSCs through the phosphorylation of SPRY2 (28), a protein that influences receptor turnover through the sequestering of the ubiquitin ligase C-CBL (38). To assess whether similar effects were produced in GBM cells, SPRY2 was overexpressed in GBM-TICs (Figure 8A), and the effect of DYRK1A kinase inhibition was analyzed for clonal growth and EGFR stability. The influence of harmine on EGFR turnover was significantly impaired in the cells overexpressing SPRY2 (Figure 8B), suggesting that DYRK1A functions upstream of this protein. More importantly, SPRY2 expression reversed the suppression of self-renewal induced by harmine (Figure 8C), demonstrating that DYRK1A controls GBM-TIC self-renewal by maintaining higher levels of EGFR at the membrane and inhibiting the termination of its downstream signal.

Discussion

Mutations and/or overexpression of EGFR are the most common alterations in GBMs, and they have been associated with tumor initiation and growth, as well as with resistance to chemo- and radiotherapy (39, 40). However, though EGFR kinase inhibitors are useful in treating other types of tumors, they offer poor results in GBM patients. Moreover, the type of EGFR mutations in GBMs often involve deletions in the extracellular domain or cytoplasmic tail, whereas mutations in the kinase domain that are commonly found in lung cancer, for example, are rare in GBMs (41). These results underline the special nature of the EGFR oncogenic network in these neoplasms and suggest that alternative strategies must be adopted to effectively target this signaling pathway in high-grade gliomas. Our data indicate that DYRK1A is a key therapeutic target for a subset of GBMs (those that are EGFR dependent), and we demonstrate that DYRK1A inhibition increases the amount of EGFR targeted for degradation, which causes a large percentage of GBM-TICs to lose their self-renewal potential in vitro and their tumorigenic capacity in vivo.

Several possibilities have been proposed to explain the resistance of GBMs to EGFR inhibitors: coactivation of compensatory pathways, upregulation of escape genes, the presence of permanently active mutations (like EGFRvIII (16, 42), or the fact that first-generation TK inhibitors do not bind to the inactive EGFR conformation that is predominant in GBM cells (43, 44). Additionally, EGFR inhibition has been reported to impair GBM cell proliferation more than it impairs survival, and this effect on GBM-TICs is reversible as tumor cells recover their self-renewal capacity after drug removal (45). More recently, it was proposed that reducing EGFR levels (but

not TK inhibition) induces autophagic cancer cell death through modulation of glucose transport (46). The data presented here suggest that DYRK1A blockade exerts an irreversible effect on GBM cells, since they lose their clonogenic capacity even after removing the pharmacological inhibitors or the shRNA inducer. Without ruling out the possibility that DYRK1A affects other signaling pathways in the GBM-TICs, our data show that the blockade inhibits EGFR stability, and therefore targeting EGFR for degradation could be more effective than inhibiting its kinase activity. In fact, a kinase-defective EGFR can stimulate DNA synthesis (47) and enhance cell survival (48). In this regard, it was proposed that one potential mode of action of the monoclonal antibodies directed against EGFR, which are currently undergoing phase III trials for glioma treatment, may involve their ability to target EGFR for lysosomal degradation (49). We propose that small molecules targeting DYRK1A kinase activity could be a good strategy for inhibiting EGFR stability. We used the β-carboline alkaloid harmine (32) and INDY, a benzothiazole compound (34), with harmine being able to inhibit GBM tumor growth and survival. Harmine and INDY have been shown to bind to the ATP pocket of DYRK1A and inhibit its kinase activity (50). They have limited use in vivo, however, as systemic INDY treatment does not reach the brain and harmine is a potent inhibitor of monoamine oxidase (35). However, molecular docking analysis showed that harmine has many degrees of freedom in the ATP-binding pocket of DYRK1A and that this could be exploited to more selectively inhibit the kinase (50).

Our data support the notion that maintaining high levels of EGFR at the membrane is a key oncogenic event, at least in a subset of GBMs. EGFR (also called ErbB1) belongs to the family of ErbB proteins, whose members differ in their signaling potency depending on distinct mechanisms that negatively regulate the receptor's fate. For example, only EGFR is strongly coupled to the C-CBL adaptor protein, and unlike other ErbB members, it is effectively targeted for lysosomal degradation (51). Impaired endocytic downregulation of receptors is frequently associated with cancer. Indeed, dominant-negative forms of *CBL* are found as oncogenes in human myeloid neoplasms (52). However, no such mutations have been found in GBMs, although the 19q13 allele containing *C-CBL* is frequently lost in these tumors (53). More recently, the transmembrane glycoprotein LRIG1 has been found to be attenuated in many astrocytomas and to control CBL recruitment and EGFR downregulation (54); also, LRIG1, which controls CBL recruitment and EGFR downregulation, has been found to be attenuated in many astrocytomas (54). Likewise, a molecule that targets EGFR to lysosomal degradation, MIG6, inhibits anchorage-independent GBM growth and is frequently deleted in these tumors (56). Thus, like DYRK1A inhibition, upregulation of LRIG1 or MIG6 limits the activation of EGFR and causes a strong inhibition of GBM-TIC self-renewal in vitro and impairs tumor survival in vivo, which reinforces the therapeutic potential of targeting EGFR stability in a subset of GBMs.

Our biochemical results suggest that DYRK1A functions upstream of SPRY2 to modulate EGFR lysosomal targeting and GBM-TIC self-renewal. These results are consistent with our previous findings in normal neural progenitors (28). SPRY2 belongs to a family of growth factor–mediated mitogen-activated protein kinase (MAPK) modulators. Paradoxically, SPRY2 also exerts a positive effect on EGFR signaling through its interaction with proteins like C-CBL and the hepatocyte growth factor–regulated tyrosine kinase substrate (HRS), which are involved in the endocytosis and degradation of EGFR (38). Phosphorylation of SPRY2 on THR75 by DYRK1A dampens its inhibitory influence on FGF-induced MAPK activation (57). This phosphorylation could potentially regulate SPRY2 binding to regulatory proteins and help discriminate between the EGF and FGF signaling pathways, as described for other residues (58, 59). Although SPRY2 is a tumor suppressor in different types of cancer, it has a tumor-promoting activity in colon cancer (60). In GBMs, several members of the SPRY family are included in a transcriptome module that was associated with the EGFR amplification status in GBMs (61), suggesting that they could act as oncogenes in at least a subset of glial tumors. Further studies are necessary to explore the DYRK1A-SPRY2 interaction in GBMs, as well as in other types of cancers that might be EGFR dependent.

Our data illustrate that DYRK1A inhibition has a direct effect on GBM-TICs, controlling their self-renewal capacity, although there were small discrepancies between the effects of DYRK1A inhibition in vivo and in vitro. There was a clear blocking of proliferation and the appearance of apoptotic cells in mouse xenografts after DYRK1A suppression, whereas no such effects were detected in the GBM-TIC cultures. DYRK1A levels have been shown to modulate the apoptosis of retinal ganglion cells during development through a regulatory phosphorylation of caspase 9 (33), and it is therefore possible that it also has a protective role in the tumor environment. Moreover, we cannot rule out the possibility that DYRK1A has a paracrine effect in tumors and that it could participate in other aspects of GBM biology, like angiogenesis. It is worth noting that harmine-containing plants have been used as traditional medicine in anticancer therapy. Furthermore, harmine has been shown to inhibit neovessel formation in vitro and in vivo through the regulation of several angiogenic factors and inflammatory cytokines (62). Although it is not known if DYRK1A is the direct mediator of such effects, future studies are needed to ascertain the role of DYRK1A in apoptosis or tumor vessel formation in glial tumors and whether its activity involves EGFR stability.

In recent years, much effort has been made to elucidate the molecular alterations in GBMs and has resulted in a large number of novel, targeted molecular therapies. However, none of these has translated into clinical benefits. The case of EGFR is an exemplary one, in that the therapeutic response was minimal despite the high expectations that EGFR kinase inhibitors would provide important clinical benefits. Here, we propose that recovery of EGFR stability (more than kinase activity per se) is an essential oncogenic event in a large percentage of GBMs. Several molecules can modulate the cell surface expression of EGFR, but none of them can be as easily targeted as DYRK1A. Therefore, targeting this kinase with small molecules, alone or in combination with EGFR inhibitors or DNA-damaging agents, could be extremely beneficial in treating EGFR-dependent GBMs.

Methods

Patients and tumor samples

Samples from patients diagnosed with brain tumors were provided by the Hospital de Madrid Tumor Bank Network, Hospital Universitario 12 de Octubre (Madrid, Spain) and Hospital Universitario La Fe (Valencia, Spain).

Primary lines and culture conditions

GBM1, GBM2, and GBM3 were obtained by cell dissociation of human GBM surgical specimens from patients treated at the "Hospital 12 de Octubre" (Madrid, Spain). Fresh tissue samples were digested enzymatically using Accumax (Millipore), and the isolated cells were purified by a

Ficoll gradient (GE Healthcare) and plated at a density of 50,000 cells per milliliter in culture medium consisting of Neurobasal (Invitrogen) supplemented with B27 (1:50) (Invitrogen); GlutaMAX (1:100) (Invitrogen); penicillin-streptomycin (1:100:Lonza); 0.4% heparin (Sigma-Aldrich); and 40 ng/ml EGF and 20 ng/ml $bFGF_2$ (complete medium; Peprotech). The GBM4, GBM5, and GBM6 primary lines were provided by Rosella Galli (San Raffaele Scientific Institute, Milan, Italy) (19), while the U87, U373, and LN18 cell lines were obtained from the ATCC. All human cell lines were grown in complete medium and were passaged after enzymatic disaggregation using Accumax (Millipore). Mouse SVZ primary neural stem cell cultures were obtained as described previously (63) and cultured in complete medium supplemented with 20 ng/ml EGF and 10 ng/ml $bFGF_2$.

Reagents

Harmine hydrochloride (TCI Europe) and INDY (34) were resuspended in water and DMSO, respectively. They were used at a final concentration of 20 μM unless otherwise noted. PCR primers and antibodies used throughout the study are listed in Supplemental Tables 1 and 2.

Retroviral and lentiviral vectors

The lentiviral vectors pLKO.1-shRNASCRAMBLE and pLKOsh*DYRK1A* (Sigma-Aldrich) were used for the stable *DYRK1A* interference. For *DYRK1A*–inducible interference, the pTRIPZ lentiviral shRNAmir (V3THS-376671 clone) was used (Open Biosystems). Infected cells were selected with 1 μg/ml of puromycin, and shRNAmir expression was induced by 1 μg/ml of doxycycline (Sigma-Aldrich). Retroviral vectors used were: pLPCX (Clontech), pLPCX-*SPRY2* (a gift from J.M. Rojas, ISCIII, Madrid, Spain), MSCV-PIG, and MSCV-EGFRvIII (Addgene).

EGFR degradation assays

Growth factor–starved NSC and GBM cells were incubated in the presence or absence of doxycycline (12 hours) or harmine (4 hours). Cycloheximide (30 μg/ml; Sigma-Aldrich) was added to the cells and 1 hour later, EGF (100 ng/ml) was added for the indicated durations. The cells were chilled on ice and cell pellets were processed for Western blot analysis.

EGFR lysosomal targeting

Growth factor–starved primary cultures were incubated in the presence or absence of harmine (20 μM) for 3 hours. Afterwards, 100 ng/ml of Alexa Fluor 488–conjugated EGF (Invitrogen) and 50 nM of LysoTracker Red (Invitrogen) were added, and cells were incubated at 4°C for 30 minutes. The cultures were then washed twice with cold PBS and either fixed immediately ($t = 0$) or incubated at 37°C in 5% CO_2 for an additional 90 minutes to allow EGFR internalization before fixing. DAPI (0.1 μg/ml) was used to stain the nuclei. Fluorescence images were obtained on a confocal microscopy (Leica TCS SP5 AOBS) and yellow colocalization spots were quantified.

Mouse xenograft assays

Orthotopic xenografts. Stereotactically guided intracranial injections in athymic nude *Foxn1*^{nu} mice (Harlan Iberica) were performed by administering 10,000 (U87) to 50,000 (primary lines) cells resuspended in 2 μl of culture medium. The injections were made into the striatum (coordinates: A-P, –0.5 mm; M-L, +2 mm; D-V, –3 mm; related to Bregma) using a Hamilton syringe, and the animals were sacrificed at the onset of symptoms.

Heterotopic xenografts. Cells (3×10^6) were resuspended 1:1 in culture media and Matrigel (BD) and then subcutaneously injected into athymic nude *Foxn1*^{nu} mice. The tumor volume was measured with a caliper when it reached a visible size.

Mouse drug treatments

Harmine treatment. Two weeks after intracranial injection, mice were treated with harmine (15 mg/kg/day) or vehicle (saline) i.p. until they were sacrificed.

Doxycycline treatment. Mice were given 2 mg/ml doxycycline in their drinking water at the indicated times.

Statistics

A Kruskal-Wallis test was used to analyze the expression of *DYRK1A* and *EGFR* in the human samples. A Spearman's correlation test was used to assess the relationship between the expression of *DYRK1A* and *EGFR*. The survival of nude mice was analyzed by the Kaplan-Meier method and evaluated with a 2-sided log-rank test. A 2-tailed Student's *t* test was performed for statistical analysis of the in vitro studies. The data in the graphs are presented as the means ± SEM. $^*P \le 0.05$; $^{**}P \le 0.01$; $^{***}P \le 0.001$. Statistical values of $P > 0.05$ were not considered significant.

Study approval

The present studies with animals and human samples were reviewed and approved by the Research Ethics and Animal Welfare Committee at the Instituto de Salud Carlos III, Madrid, in agreement with the European Union and national directives. The human tissues were procured after obtaining the patients' written consent and with the approval of the ethics committees of each participating hospital (Clinical Research Ethics Committee from Hospital Universitario 12 de Octubre, Madrid; Hospital Universitario La Fe, Valencia; and Hospital de Madrid, Madrid).

Further information can be found in the Supplemental Methods.

Acknowledgments

We thank R. Galli for providing the primary GBM lines, J.M.Rojas for providing the SPRY2 plasmids, and S. de la Luna and A. Ruiz i Altaba for helpful comments. We also thank R. Pérez and F. González for helping with the mouse histology and confocal images, respectively. This work was supported by grants from the Ministerio de Educación y Ciencia (MEC; SAF2008-04531), the Ministerio de Ciencia e Innovación (MICINN, PLE2009-0115), and the Ministerio de Asuntos Exteriores y Cooperación (MAEC-AECID A/023963/09; to P. Sánchez-Gómez), as well as by grants from the Fondo de Investigación Sanitaria (FIS-PS09-01977) and Fundación Mutua-madrileña grants (FMM 2007/057, to J.R. Ricoy; and FMM2011/89, to J.M. Sepúlveda).

Received for publication January 30, 2013, and accepted in revised form March 1, 2013.

Address correspondence to: Pilar Sánchez-Gómez, Instituto de Salud Carlos III-UFIEC, Neuro-oncology Unit, Crtra. Majadahonda-Pozuelo, Km 2, Majadahonda, UNK 28922, Spain. Phone: 34918223265; Fax: 34918223269; E-mail: psanchezg@isciii.es.

1. Louis DN, Ohgaki H, Wiestler OD, Cavenee WK. *WHO Classification of Tumours of the Central Nervous System*. 4th ed. Lyon, France: International Agency for Research on Cancer; 2007.
2. Stupp R, et al. Radiotherapy plus concomitant and adjuvant temozolomide for glioblastoma. *N Engl J Med*. 2005;352(10):987–996.
3. Chamberlain MC. Emerging clinical principles on the use of bevacizumab for the treatment of malignant gliomas. *Cancer*. 2010;116(17):3988–3999.
4. Singh SK, et al. Identification of human brain tumour initiating cells. *Nature*. 2004; 432(7015):396–401.
5. Galli R, et al. Isolation and characterization of tumorigenic, stem-like neural precursors from human glioblastoma. *Cancer Res*. 2004;64(19):7011–7021.
6. Yuan X, et al. Isolation of cancer stem cells from adult glioblastoma multiforme. *Oncogene*. 2004; 23(58):9392–9400.
7. Sutter R, Yadirgi G, Marino S. Neural stem cells, tumour stem cells and brain tumours: danger-

ous relationships? *Biochim Biophys Acta.* 2007; 1776(2):125–137.
8. Nicolis SK. Cancer stem cells and "stemness" genes in neuro-oncology. *Neurobiol Dis.* 2007;25(2):217–229.
9. Dirks PB. Brain tumor stem cells: the cancer stem cell hypothesis writ large. *Mol Oncol.* 2010;4(5):420–430.
10. Lee J, et al. Tumor stem cells derived from glioblastomas cultured in bFGF and EGF more closely mirror the phenotype and genotype of primary tumors than do serum-cultured cell lines. *Cancer Cell.* 2006;9(5):391–403.
11. Bao S, et al. Glioma stem cells promote radioresistance by preferential activation of the DNA damage response. *Nature.* 2006;444(7120):756–760.
12. Beier D, Schulz JB, Beier CP. Chemoresistance of glioblastoma cancer stem cells — much more complex than expected. *Mol Cancer.* 2011;10:128.
13. Wang R, et al. Glioblastoma stem-like cells give rise to tumour endothelium. *Nature.* 2010; 468(7325):829–833.
14. Ricci-Vitiani L, et al. Tumour vascularization via endothelial differentiation of glioblastoma stem-like cells. *Nature.* 2010;468(7325):824–828.
15. Stiles CD and Rowitch DH. Glioma stem cells: a midterm exam. *Neuron.* 2008;58(6):832–846.
16. Lo HW. EGFR-targeted therapy in malignant glioma: novel aspects and mechanisms of drug resistance. *Curr Mol Pharmacol.* 2010;3(1):37–52.
17. Soeda A, et al. Epidermal growth factor plays a crucial role in mitogenic regulation of human brain tumor stem cells. *J Biol Chem.* 2008;283(16):10958–10966.
18. Jin X, et al. EGFR-AKT-Smad signaling promotes formation of glioma stem-like cells and tumor angiogenesis by ID3-driven cytokine induction. *Cancer Res.* 2011;71(22):7125–7134.
19. Mazzoleni S, et al. Epidermal growth factor receptor expression identifies functionally and molecularly distinct tumor-initiating cells in human glioblastoma multiforme and is required for gliomagenesis. *Cancer Res.* 2010;70(19):7500–7513.
20. Raizer JJ. HER1/EGFR tyrosine kinase inhibitors for the treatment of glioblastoma multiforme. *J Neurooncol.* 2005;74(1):77–86.
21. Peereboom DM, et al. Phase II trial of erlotinib with temozolomide and radiation in patients with newly diagnosed glioblastoma multiforme. *J Neurooncol.* 2010;98(1):93–99.
22. van den Bent MJ, et al. Randomized phase II trial of erlotinib versus temozolomide or carmustine in recurrent glioblastoma: EORTC brain tumor group study 26034. *J Clin Oncol.* 2009;27(8):1268–1274.
23. Mellinghoff IK, et al. Molecular determinants of the response of glioblastomas to EGFR kinase inhibitors. *N Engl J Med.* 2005;353(19):2012–2024.
24. Haas-Kogan DA, et al. Epidermal growth factor receptor, protein kinase B/Akt, and glioma response to erlotinib. *J Natl Cancer Inst.* 2005; 97(12):880–887.
25. Aranda S, Laguna A, de la LS. DYRK family of protein kinases: evolutionary relationships, biochemical properties, and functional roles. *FASEB J.* 2011; 25(2):449–462.
26. Tejedor FJ and Hammerle B. MNB/DYRK1A as a multiple regulator of neuronal development. *FEBS J.* 2011;278(2):223–235.
27. Wegiel J, Gong CX, Hwang YW. The role of DYRK1A in neurodegenerative diseases. *FEBS J.* 2011; 278(2):236–245.
28. Ferron SR, et al. Regulated segregation of kinase Dyrk1A during asymmetric neural stem cell division is critical for EGFR-mediated biased signaling. *Cell Stem Cell.* 2010;7(3):367–379.
29. Marti E, et al. Dyrk1A expression pattern supports specific roles of this kinase in the adult central nervous system. *Brain Res.* 2003;964(2):250–263.
30. Wegiel J, et al. Cell type- and brain structure-specific patterns of distribution of minibrain kinase in human brain. *Brain Res.* 2004;1010(1–2):69–80.
31. Reifenberger J, Reifenberger G, Ichimura K, Schmidt EE, Wechsler W, Collins VP. Epidermal growth factor receptor expression in oligodendroglial tumors. *Am J Pathol.* 1996;149(1):29–35.
32. Bain J, et al. The selectivity of protein kinase inhibitors: a further update. *Biochem J.* 2007;408(3):297–315.
33. Laguna A, et al. The protein kinase DYRK1A regulates caspase-9-mediated apoptosis during retina development. *Dev Cell.* 2008;15(6):841–853.
34. Ogawa Y, et al. Development of a novel selective inhibitor of the Down syndrome-related kinase Dyrk1A. *Nat Commun.* 2010;1:86.
35. Coates GH, Cox B. Harmine tremor after brain monoamine oxidase inhibition in the mouse. *Eur J Pharmacol.* 1972;18(2):284–286.
36. Pandita A, Aldape KD, Zadeh G, Guha A, James CD. Contrasting in vivo and in vitro fates of glioblastoma cell subpopulations with amplified EGFR. *Genes Chromosomes Cancer.* 2004;39(1):29–36.
37. Ramnarain DB, et al. Differential gene expression analysis reveals generation of an autocrine loop by a mutant epidermal growth factor receptor in glioma cells. *Cancer Res.* 2006;66(2):867–874.
38. Cabrita MA, Christofori G. Sprouty proteins, masterminds of receptor tyrosine kinase signaling. *Angiogenesis.* 2008;11(1):53–62.
39. Karpel-Massler G, Schmidt U, Unterberg A, Halatsch ME. Therapeutic inhibition of the epidermal growth factor receptor in high-grade gliomas: where do we stand? *Mol Cancer Res.* 2009;7(7):1000–1012.
40. Squatrito M, Holland EC. DNA damage response and growth factor signaling pathways in gliomagenesis and therapeutic resistance. *Cancer Res.* 2011; 71(18):5945–5949.
41. Frederick L, Wang XY, Eley G, James CD. Diversity and frequency of epidermal growth factor receptor mutations in human glioblastomas. *Cancer Res.* 2000;60(5):1383–1387.
42. Wheeler DL, Dunn EF, Harari PM. Understanding resistance to EGFR inhibitors-impact on future treatment strategies. *Nat Rev Clin Oncol.* 2010; 7(9):493–507.
43. Vivanco I, et al. Differential sensitivity of glioma- versus lung cancer-specific EGFR mutations to EGFR kinase inhibitors. *Cancer Discov.* 2012; 2(5):458–471.
44. Barkovich KJ, et al. Kinetics of inhibitor cycling underlie therapeutic disparities between EGFR-driven lung and brain cancers. *Cancer Discov.* 2012;2(5):450–457.
45. Jun HJ, et al. Acquired MET expression confers resistance to EGFR inhibition in a mouse model of glioblastoma multiforme. *Oncogene.* 2012; 31(25):3039–3050.
46. Weihua Z, et al. Survival of cancer cells is maintained by EGFR independent of its kinase activity. *Cancer Cell.* 2008;13(5):385–393.
47. Coker KJ, Staros JV, Guyer CA. A kinase-negative epidermal growth factor receptor that retains the capacity to stimulate DNA synthesis. *Proc Natl Acad Sci U S A.* 1994;91(15):6967–6971.
48. Ewald JA, Wilkinson JC, Guyer CA, Staros JV. Ligand- and kinase activity-independent cell survival mediated by the epidermal growth factor receptor expressed in 32D cells. *Exp Cell Res.* 2003; 282(2):121–131.
49. Friedman LM, et al. Synergistic down-regulation of receptor tyrosine kinases by combinations of mAbs: implications for cancer immunotherapy. *Proc Natl Acad Sci U S A.* 2005;102(6):1915–1920.
50. Adayev T, Wegiel J, Hwang YW. Harmine is an ATP-competitive inhibitor for dual-specificity tyrosine phosphorylation-regulated kinase 1A (Dyrk1A). *Arch Biochem Biophys.* 2011; 507(2):212–218.
51. Levkowitz G, et al. c-Cbl/Sli-1 regulates endocytic sorting and ubiquitination of the epidermal growth factor receptor. *Genes Dev.* 1998;12(23):3663–3674.
52. Kales SC, Ryan PE, Nau MM, Lipkowitz S. Cbl and human myeloid neoplasms: the Cbl oncogene comes of age. *Cancer Res.* 2010;70(12):4789–4794.
53. Mizoguchi M, Nutt CL, Louis DN. Mutation analysis of CBL-C and SPRED3 on 19q in human glioblastoma. *Neurogenetics.* 2004;5(1):81–82.
54. Guo D, et al. Perinuclear leucine-rich repeats and immunoglobulin-like domain proteins (LRIG1-3) as prognostic indicators in astrocytic tumors. *Acta Neuropathol.* 2006;111(3):238–246.
55. Ye F, et al. Upregulation of LRIG1 suppresses malignant glioma cell growth by attenuating EGFR activity. *J Neurooncol.* 2009;94(2):183–194.
56. Ying H, et al. Mig-6 controls EGFR trafficking and suppresses gliomagenesis. *Proc Natl Acad Sci U S A.* 2010;107(15):6912–6917.
57. Aranda S, Alvarez M, Turro S, Laguna A, de la LS. Sprouty2-mediated inhibition of fibroblast growth factor signaling is modulated by the protein kinase DYRK1A. *Mol Cell Biol.* 2008;28(19):5899–5911.
58. Kim HJ, Taylor LJ, Bar-Sagi D. Spatial regulation of EGFR signaling by Sprouty2. *Curr Biol.* 2007; 17(5):455–461.
59. Rubin C, Zwang Y, Vaisman N, Ron D, Yarden Y. Phosphorylation of carboxyl-terminal tyrosines modulates the specificity of Sprouty-2 inhibition of different signaling pathways. *J Biol Chem.* 2005; 280(10):9735–9744.
60. Barbachano A, et al. SPROUTY-2 and E-cadherin regulate reciprocally and dictate colon cancer cell tumourigenicity. *Oncogene.* 2010;29(34):4800–4813.
61. Ivliev AE, 't Hoen PA, Sergeeva MG. Coexpression network analysis identifies transcriptional modules related to proastrocytic differentiation and sprouty signaling in glioma. *Cancer Res.* 2010; 70(24):10060–10070.
62. Hamsa TP, Kuttan G. Harmine inhibits tumour specific neo-vessel formation by regulating VEGF, MMP, TIMP and pro-inflammatory mediators both in vivo and in vitro. *Eur J Pharmacol.* 2010; 649(1–3):64–73.
63. Ferron SR, Andreu-Agullo C, Mira H, Sanchez P, Marques-Torrejon MA, Farinas I. A combined ex/in vivo assay to detect effects of exogenously added factors in neural stem cells. *Nat Protoc.* 2007; 2(4):849–859.

Molecular Vision 2013; 19:536-543 <http://www.molvis.org/molvis/v19/536>
Received 4 July 2012 | Accepted 2 March 2013 | Published 5 March 2013

Specific inhibition of serine/arginine-rich protein kinase attenuates choroidal neovascularization

Zhenyu Dong,[1,2] Kousuke Noda,[1,2] Atsuhiro Kanda,[1,2] Junichi Fukuhara,[1,2] Ryo Ando,[1,2] Miyuki Murata,[1,2] Wataru Saito,[1] Masatoshi Hagiwara,[3] Susumu Ishida[1,2]

[1]Department of Ophthalmology, Hokkaido University Graduate School of Medicine, Sapporo, Japan; [2]Laboratory of Ocular Cell Biology and Visual Science, Hokkaido University Graduate School of Medicine, Sapporo, Japan; [3]Department of Anatomy and Developmental Biology, Kyoto University Graduate School of Medicine, Kyoto, Japan

Purpose: To investigate the applicability of serine/arginine-rich protein kinase (SRPK)-specific inhibitor, SRPIN340, for attenuation of choroidal neovascularization (CNV) formation using a mouse model.
Methods: Laser photocoagulation was performed to induce CNV in C57BL/6J mice, followed by intravitreal injection of SRPIN340 or vehicle. Seven days after the treatment, the CNV size was evaluated using a flatmount technique. Protein levels of vascular endothelial growth factor (VEGF) and inflammation-associated molecules, such as monocyte chemoattractant protein (MCP)-1 and intercellular adhesion molecule (ICAM)-1, in the retinal pigment epithelium-choroid complex were measured with enzyme-linked immunosorbent assay. Expression levels of total *Vegf*, exon 8a-containing *Vegf* isoforms, and *F4/80* (a specific marker for macrophage) were assessed using real-time PCR.
Results: SRPIN340 inhibited CNV formation in a dose-dependent manner. Compared with the vehicle, SRPIN340 significantly decreased the protein levels of VEGF, MCP-1, ICAM-1, and consequently inhibited macrophage infiltration. Furthermore, SRPIN340 suppressed the gene expression levels of total *Vegf* and exon 8a-containing *Vegf* isoforms.
Conclusions: SRPIN340, a specific inhibitor of SRPK, suppressed *Vegf* expression and attenuated CNV formation. Our data suggest the possibility that SRPIN340 is applicable for neovascular age-related macular degeneration as a novel chemical therapeutics.

Age-related macular degeneration (AMD) is the primary cause of visual loss in developed countries [1-3]. In particular, neovascular AMD, characterized by choroidal neovascularization (CNV), is responsible for most cases of severe vision loss due to AMD [4,5]. CNV formation occurs through multifactorial processes involving the complex interaction of metabolic, genetic, and environmental factors. In particular, recent basic [6, 7] and clinical [8-10] investigations have provided strong evidence that growth factors and cytokines, such as vascular endothelial growth factor (VEGF), play a pivotal role in the process of pathological angiogenesis.

The cytokine VEGF had long been considered a proangiogenic factor, but Bates and his colleagues identified antiangiogenic *VEGF* isoforms, *VEGFxxxb* (xxx denotes the number of amino acids), generated as a result of distal splice site selection in exon 8 (i.e., exon 8b) during alternative splicing of *VEGF* messenger RNA precursor (pre-mRNA) [11]. Pro- and antiangiogenic *VEGF* isoforms are generated from the same *VEGF* gene via alternative splicing of mRNA. The alternative splicing of *VEGF* pre-mRNA is regulated by splicing regulatory factors, including various serine/arginine-rich (SR) proteins [12]. Previous studies have shown that SR protein kinase (SRPK) activates SRSF1 (SF2/ASF) and SRSF5 (SRp40), both of which favor splicing site selection at exon 8a during the splicing of *VEGF* pre-mRNA, and consequently lead to upregulation of proangiogenic *VEGF* isoforms [13]. We have developed a specific inhibitor for SRPK, SRPIN340 [14], and inhibition of SRPK with SRPIN340 suppressed retinal angiogenesis by reducing the ratio of proangiogenic to total *VEGF* isoforms at the mRNA level [15]. In this study, we investigated the therapeutic effect of SRPIN340 on CNV using the laser photocoagulation model and found that SRPIN340 suppressed *Vegf* expression and attenuated CNV formation.

Correspondence to: Kousuke Noda, Department of Ophthalmology, Hokkaido University Graduate School of Medicine, N7, W15, Kita-ku, Sapporo, Hokkaido 060-8638, Japan; Phone: 81-11-706-5943; Fax: 81-11-706-5948; email: nodako@med.hokudai.ac.jp

METHODS

Animals and induction of choroidal neovascularization: Eight-week-old C57BL/6J male mice (CLEA Japan, Tokyo, Japan) were used for this study. All animal experiments were approved by the Hokkaido University Animal Use Committee and conducted in accordance with the Association for Research in Vision and Ophthalmology Statement for the Use of Animals in Ophthalmic and Vision Research. Anesthesia was induced by intraperitoneal injection of pentobarbital (0.05 mg/g bodyweight), and pupils were dilated with

topical 5% phenylephrine hydrochloride and 5% tropicamide. After anesthesia induction and pupil dilation, four laser spots were placed around the optic disc (532 nm, 200 mW power, 0.1 s, 75 µm spot size, Novus Spectra; Lumineis, Tokyo, Japan) using a slit-lamp delivery system with a cover glass as a contact lens. Laser spots with vitreous, retinal, or subretinal hemorrhage were excluded from the analysis.

Serine/arginine-rich protein kinase inhibitor: SRPIN340, an isonicotinamide compound, N-[2-(1-piperidinyl)-5-(trifluoromethyl)phenyl] (Figure 1), was found in a screening for chemicals specifically inhibiting SRPK to suppress the acute replication of viruses such as human immunodeficiency virus, using a scintillation proximity assay with a synthetic RS-repeat peptide as the substrate [16]. For SRPKs, SRPIN340 selectively inhibits SRPK1 and SRPK2 but does not inhibit other classes of SRPKs significantly, including Clk1 and Clk4 [14].

SRPIN340 treatment: SRPIN340 (50 mM in 100% dimethyl sulfoxide, DMSO) was diluted with phosphate buffered saline (PBS, potassium chloride, 2.68 mM; potassium phosphate monobasic, 1.47 mM; sodium chloride, 136.89 mM; sodium phosphate dibasic, 8.10 mM) to various concentrations in 0.1% DMSO before treatment. Mice were divided into five groups: CNV induction alone (the control group) and CNV induction with 1 µl intravitreal injection of either 0.1% DMSO, 0.2 pmol, 2 pmol, or 20 pmol SRPIN340. Intravitreal injection was performed using a 33-gauge needle (Extreme Microsyringe, Ito Corporation, Tokyo, Japan) immediately after laser photocoagulation.

Measurement of choroidal neovascularization: Seven days after laser injury, mice were euthanized with an overdose of anesthesia, performed by intraperitoneal injection with 2 mL of 5% pentobarbital sodium, and perfused with 5 mL PBS through the left ventricle, followed by 2.5 mL of 0.5% fluorescein-isothiocyanate-labeled dextran (Sigma-Aldrich, St. Louis, MO) in 1% gelatin. Subsequently, the eyes were enucleated and fixed with 2% paraformaldehyde for 30 min.

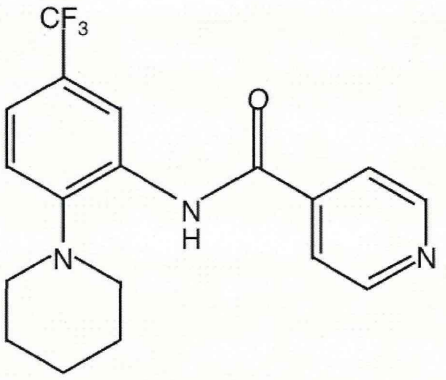

Figure 1. Structure of SRPIN340.

Flat mounts of retinal pigment epithelium (RPE)-choroid complex were obtained by removing the anterior segments and the neural retina. Four to six radial relaxing incisions were made to allow the residual posterior eyecup to be laid flat. After mounting with the Vectashield Mounting Medium (Vector Laboratories, Burlingame, CA) and coverage with a coverslip, the flat mounts were examined with a fluorescence microscope (Biorevo, Keyence, Tokyo, Japan), and the CNV area was measured and used for the evaluation.

RNA extraction and real-time polymerase chain reaction: Total RNA was extracted from the RPE-choroid complex 3 days after the laser photocoagulation procedure combined with intravitreal injection of either 1 µl of 0.1% DMSO or SRPIN340, following euthanasia by intraperitoneal injection of overdose pentobarbital (0.15 mg/g bodyweight) using TRIzol Reagent (Life Technologies, Carlsbad, CA). Reverse transcription was performed with GoScrip Reverse Transcriptase (Promega, Madison, WI) and oligo dT(20) primers following the manufacturer's instructions. The primers used in this study are summarized in Table 1 [15]. The TaqMan probe for *F4/80* was purchased from Life Technologies. Real-time PCR was performed using the GoTaq qPCR Master Mix (Promega), THUNDERBIRD Probe qPCR Mix (TOYOBO, Tokyo, Japan), and StepOnePlus Real-Time PCR System

Table 1. Primer sequences.

Gene	Sequence (5'-3')
Vegf	F: AAGGAGAGCAGA AGTCCCATGA
	R: CTCAATCGGACGGCAGTAGCT
Vegf containing exon 8a	F: GTTCAGAGCGGAGAAAGCAT
	R: TCACATCTGCAAGTACGTTCG
Actb	F: CATCCGTAAAGACCTCTATGCCAAC
	R: ATGGAGCCACCGATCCACA

Vegf, vascular endothelial growth factor; *Actb*, beta-actin

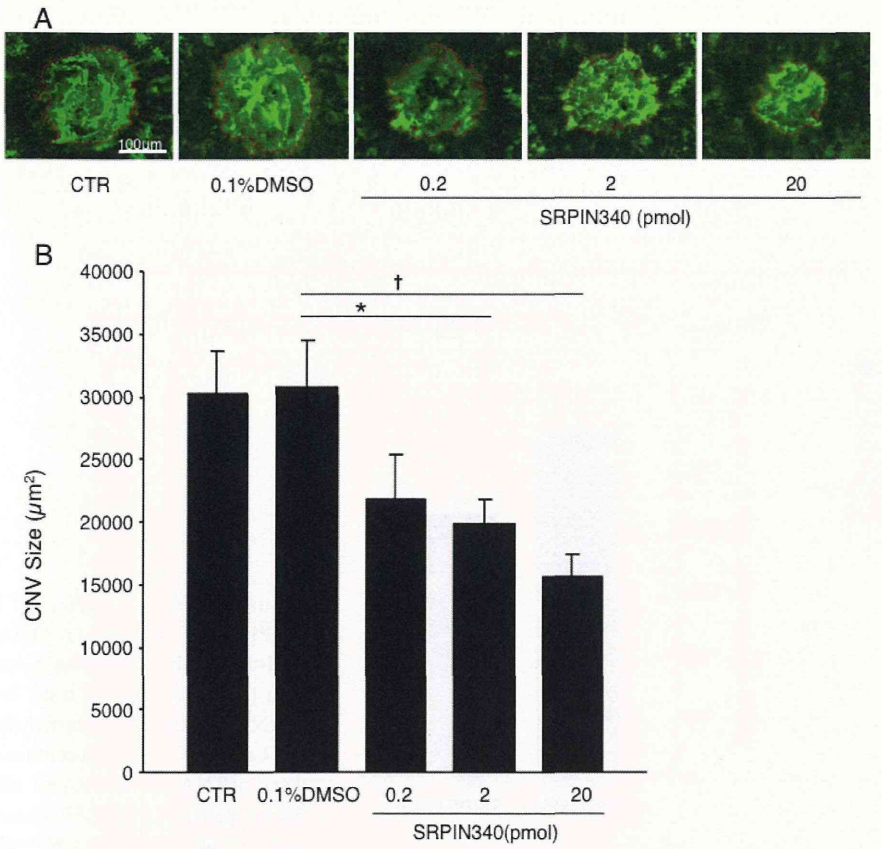

Figure 2. Suppression of choroidal neovascularization formation by SRPIN340. **A**: Representative micrographs of choroidal neovascularization (CNV) lesions in the choroidal flat mounts from mice treated with laser photocoagulation alone as control (CTR, n=32; n represents the number of CNV lesions), combined with intravitreal injection of 0.1% DMSO (n=31) or 0.2 pmol (n=17), 2 pmol (n=33), and 20 pmol (n=23) SRPIN340, respectively. **B**: Quantitative analysis of CNV size. Bars indicate the average of CNV size in each group. Values are mean±SEM. *, $p<0.05$; †, $p<0.01$.

(Life Technologies). *Actb* was used as endogenous control. Threshold cycle (C_T) was determined automatically, and relative change in mRNA expression was calculated using the ΔΔCT values as previously reported [17]. All PCR reactions were repeated in triplicate, and the average values were used in the statistical analysis.

Quantification of infiltrating macrophages: Immunostaining of F4/80 was also performed to further quantify the infiltration of macrophages. Briefly, eyes were enucleated 3 days after the laser photocoagulation in combined with 1 μl intravitreal injection of either 0.1% DMSO or 20 pmol SRPIN340, and whole choroid-sclera complexes were incubated overnight at 4 °C with a rabbit polyclonal antibody against mouse CD31 (1:100 dilution; Abcam, Tokyo, Japan) and a rat polyclonal antibody against F4/80 (1:100 dilution; Serotec, Oxford, UK) as primary antibodies, respectively. Binding of primary antibody was localized with Alexa Fluor 488 goat anti-rabbit and Alexa Fluor 546 goat anti-rat secondary antibody (1:200 dilution, respectively; Life Technologies). Finally, slides were mounted with Vectashield Mounting Medium (Vector Laboratories), and CNV was viewed with a fluorescence microscope (Biorevo, Keyence). The CD31-stained area of CNV and F4/80-positive macrophages were evaluated, and the area-adjusted number of macrophages per 1,000 μm² area of CNV was calculated.

Enzyme-linked immunosorbent assay: Four laser lesions were placed in each eye, and an intravitreal injection of either 1 μl of 0.1% DMSO or SRPIN340 was also administered. Protein levels of VEGF, monocyte chemoattractant protein (MCP)-1, and intercellular adhesion molecule (ICAM)-1 in supernatant were determined using enzyme-linked immunosorbent assay kits (R&D Systems, Minneapolis, MN) and normalized to total protein (BCA Protein Assay Kit, Thermo Scientific, Rockford, IL), according to the manufacturer's protocols.

Statistics: Results are presented as mean±standard error of the mean (SEM). Statistical analysis was performed using the two-tailed unpaired Student *t*-test, and results were considered statistically significant when the p value was less than 0.05.

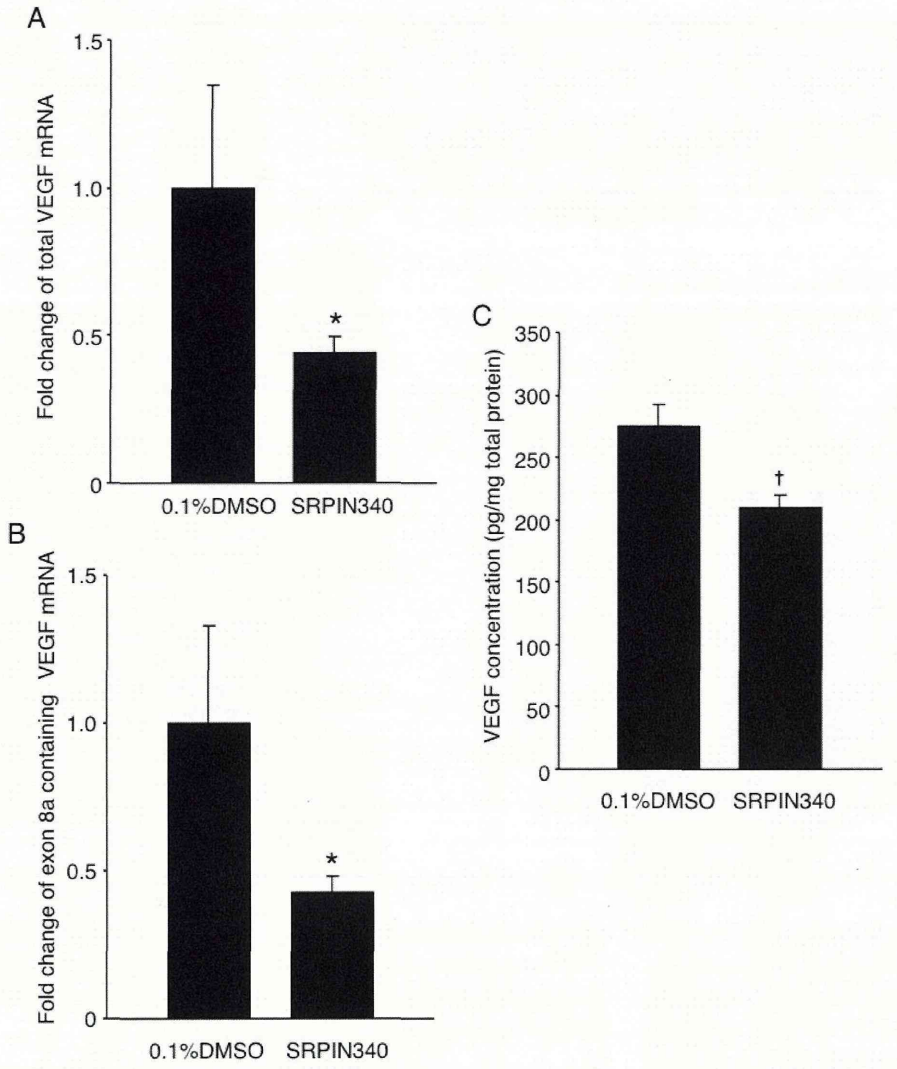

Figure 3. Inhibition of *Vegf* by SRPIN340. **A**: Bars represent real-time polymerase chain reaction (PCR) analysis of total *Vegf* mRNA. **B**: Bars represent real-time PCR analysis of exon 8a containing *Vegf* mRNA. **C**: ELISA of total VEGF protein in the RPE-choroid complex obtained from CNV mice 3 days after laser photocoagulation with intravitreal injection of 0.1% DMSO or 20 pmol SRPIN340 (n=6 to 8 for real-time PCR analysis, n=8 to 10 for ELISA, respectively; n represents the number of eyes). *, $p<0.05$; †, $p<0.01$.

RESULTS

Impact of serine/arginine-rich protein kinase blockade during choroidal neovascularization formation: To determine whether SRPK blockade inhibits CNV formation, we quantified the CNV size in the flat mounts of the RPE-choroid complex with or without SRPIN340 administration. Seven days after laser injury, the animals treated with 2 pmol SRPIN340 (n=33; n represents the number of CNV lesions) showed a significant decrease in the average CNV size (19,870±1935 μm^2), compared with the vehicle-treated animals (30,737±3758 μm^2, n=31, $p<0.05$; Figure 2A,B). Furthermore, a higher dose administration of SRPIN340 (20 pmol; n=23) significantly reduced the CNV size (15,649±1803 μm^2, $p<0.01$) to an even greater extent than that observed in the 2 pmol SRPIN340–treated animals, whereas a lower dose administration (0.2 pmol; n=17) did not significantly inhibit CNV formation (21,741±3695 μm^2, p=0.10; Figure 2A,B). No significant difference in CNV size was observed between mice subjected to laser injury alone and those subjected to laser and intravitreal injection of vehicle solution. The data indicate that SRPK blockade suppresses CNV growth in a dose-dependent manner.

Impact of serine/arginine-rich protein kinase blockade on Vegf expression: To investigate the effect of SRPIN340 on *Vegf* isoforms, mRNA expression of total *Vegf* and *Vegf* isoforms containing exon 8a were analyzed using real-time PCR. Compared with mice treated with 0.1% DMSO (n=8; n represents the number of eyes), mRNA expression of total *Vegf* in the RPE-choroid complex obtained from mice treated with 20 pmol SRPIN340 (n=6) was significantly decreased

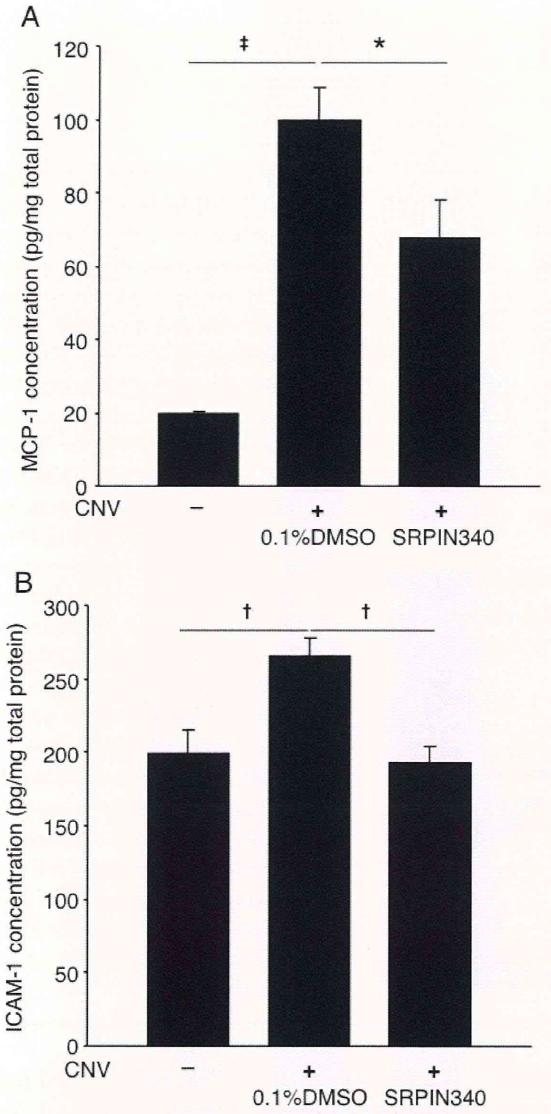

Figure 4. Reduction of inflammatory molecules by SRPIN340. **A, B**: Bars indicate average protein levels of monocyte chemoattractant protein (MCP)-1 and intercellular adhesion molecule (ICAM)-1 in the RPE-choroid complex obtained normal mice or CNV mice 3 days after laser photocoagulation combined with intravitreal injection of 0.1% DMSO or 20 pmol SRPIN340. Protein levels were measured with ELISA and normalized to total protein levels. Values are mean±SEM (n=8 to 10; n represents the number of eyes). *, $p<0.05$; †, $p<0.01$; ‡, $p<0.001$.

by 56% ($p<0.05$; Figure 3A). Similarly, mRNA expression of *Vegf* containing exon 8a was significantly decreased by 57% ($p<0.05$; Figure 3B). Furthermore, total VEGF concentration in mice treated with 20 pmol SRPIN340 (209.2±10.9 pg/mg, n=8) was significantly lower than mice treated with 0.1% DMSO (274.2±17.9 pg/mg, n=10, $p<0.01$; Figure 3C).

Suppression of adhesion molecules, inflammatory molecules, and macrophage influx by serine/arginine-rich protein kinase blockade: To explore the mechanism by which SRPIN340 suppresses CNV formation, concentrations of the inflammation-associated molecules MCP-1 and ICAM-1 in the RPE-choroid complex were measured. Levels of MCP-1 (19.5±0.9 pg/mg) and ICAM-1 (199.6±15.5 ng/mg) in the RPE-choroid complex of normal mice were significantly increased 3 days after laser photocoagulation and intravitreal injection of 0.1% DMSO (MCP-1, 99.9±8.6 pg/mg, $p<0.001$; ICAM-1, 265.4±12.3 ng/mg, $p<0.01$, respectively). However, compared with mice treated with laser photocoagulation and 0.1% DMSO, the protein levels of MCP-1 and ICAM-1 were significantly reduced in the RPE-choroid complex of the mice treated with laser photocoagulation and 20 pmol SRPIN340 (MCP-1, 67.8±10.2 pg/mg, $p<0.05$; ICAM-1, 192.9±11.6 ng/mg, $p<0.01$, n=8-10, respectively; n represents the number of eyes, Figure 4A,B).

Furthermore, real-time PCR showed that mRNA expression of *F4/80*, the marker for mouse macrophages [18], was downregulated by 41% in the animals treated with 20 pmol SRPIN340 (n=6; n represents the number of eyes) compared to that of the vehicle-treated animals (n=8, $p<0.05$; Figure 5A). In accord with the real-time PCR data, suppression of macrophage influx by SRPIN340 was also depicted in the immunofluorescence study using F4/80 antibody. Compared with the vehicle-treated animals, the number of F4/80-positive macrophages in CNV lesions significantly decreased in the animals treated with 20 pmol SRPIN340 (15.5±4.0 and 6.5±1.8 /1000 μm^2, n=13 to 15, respectively; n represents the number of CNV lesions; $p<0.05$; Figure 5B,C).

DISCUSSION

To date, intravitreal injection of anti-VEGF agents has brought revolutionary changes to the treatment of neovascular AMD. Nevertheless, novel interventions for preventing and treating neovascular AMD remain to be developed because of possible ocular and/or systemic adverse events following long-term administration [19-23]. Discovery of antiangiogenic *VEGF* isoforms highlighted the importance and necessity of differentially targeting *VEGF* isoforms in treating neovascular AMD, and suggested the possibility of regulating the splicing of *VEGF* pre-mRNA as a therapeutic strategy. Small molecules and compounds, including SRPIN340, have currently shown promising results in targeting spicing factors and kinases involved in alternative splicing [14,24,25].

Most of the findings regarding the regulation of alternative splicing of *VEGF* pre-mRNA during pathological angiogenesis were obtained from in vitro study [13,15]. Using

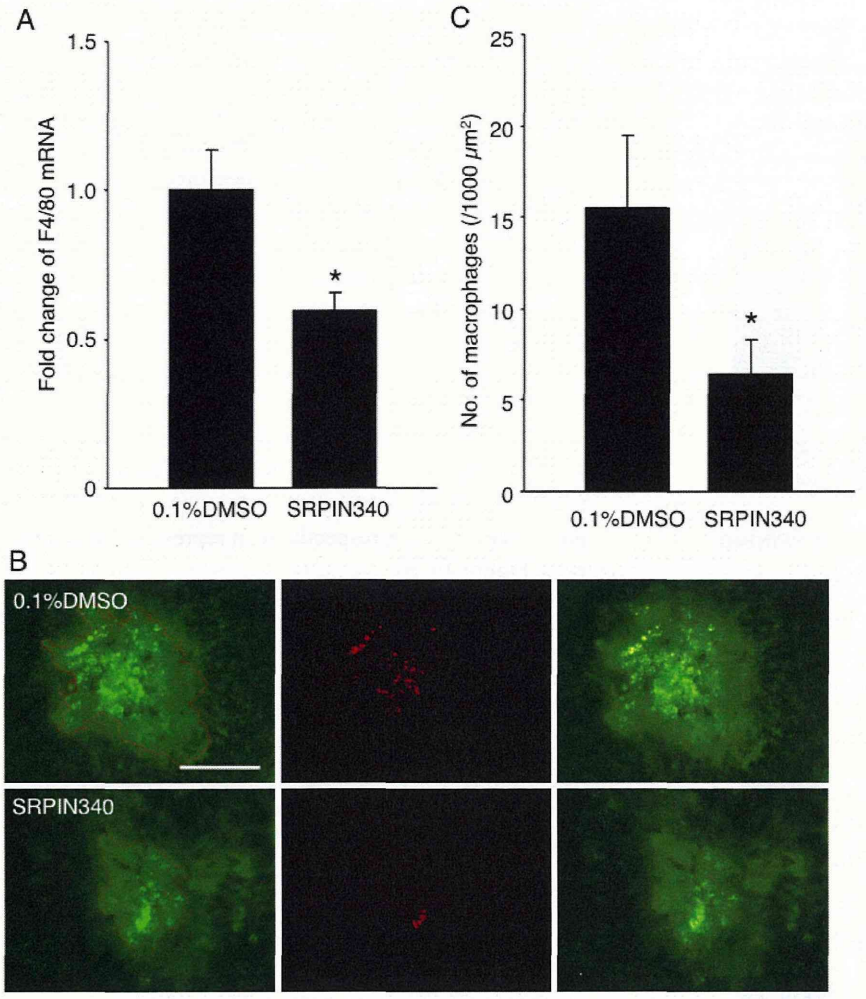

Figure 5. Inhibition of macrophage infiltration by SRPIN340. **A**: Bars represent real-time polymerase chain reaction (PCR) analysis of the relative change in *F4/80* expression in the RPE-choroid complex obtained from CNV mice 3 days after laser photocoagulation combined with intravitreal injection of 0.1% DMSO or 20 pmol SRPIN340. Values are mean±SEM (n=6 to 8; n represents the number of eyes). **B**: Micrographs depict representative *F4/80* immunostaining in CNV lesions 3 days after laser photocoagulation combined with intravitreal injection of 0.1% DMSO or 20 pmol SRPIN340. (left). CNV lesions stained for CD31 (middle). Immunofluorescence staining for F4/80 (right). Merged image. Bar, 100 μm. **C**: Quantitative analysis of F4/80-positive cells. Bars represent the average number of infiltrated macrophages in each CNV lesion. Values are mean±SEM (n=13 to 15); *n* represents the number of CNV lesions. *, $p<0.05$.

in vitro experiments, upregulation of proangiogenic *VEGF* isoforms and simultaneous downregulation of antiangiogenic *VEGF* isoforms in various pathologies have subsequently been elucidated [26-29]. In contrast, animal experiments used in investigations of this mechanism are rarely reported. Moreover, a limited number of reports are currently available on the effect of specific inhibitors for SRPK against pathological angiogenesis such as a murine hypoxia-induced retinopathy model [15] and xenotransplanted tumor growth in nude mice [30]. Previous reports suggested that this suppressive effect was caused by the upregulation of antiangiogenic *VEGF* isoforms and the subsequent restoration of the balance between pro- and antiangiogenic *VEGF* isoforms. However, our data indicated that SRPIN340 suppressed total *Vegf* and *Vegf* isoforms containing exon 8a at the mRNA level. In addition, the total VEGF protein was also decreased by the SRPK inhibitor SRPIN340. Recently, Tripathi et al. reported that SRSF1 is a component of the 7SK complex and influences RNA polymerase II-mediated transcription [31]. Since SRPK activates SRSF1 through the phosphorylation of the RS domain [32], the current data suggest that SRPK inhibition by SRPIN340 may reduce transcription of *VEGF*, in addition to the switching to antiangiogenic *VEGF* isoforms.

During CNV formation, VEGF and its related molecules reciprocally accelerate angiogenesis via macrophage infiltration. For instance, VEGF induces MCP-1 and ICAM-1 production in endothelial cells, both of which play a role in macrophage recruitment [33-35], and directly mediates macrophage migration via its receptor 1 [36]. Subsequently, the recruited macrophages secrete VEGF and facilitate CNV growth [37]. Thus, decrease of VEGF might result in reduced macrophages influx and VEGF secretion. Indeed, in the current study we observed that levels of inflammation-associated molecules were decreased during CNV formation,